

Supporting information

Intron-targeted mutagenesis reveals roles for *Dscam1* RNA pairing-mediated splicing bias in neuronal wiring

Weiling Hong¹, Haiyang Dong¹, Jian Zhang¹, Fengyan Zhou¹, Yandan Wu¹, Yang Shi¹, Shuo Chen¹, Bingbing Xu¹, Wendong You², Feng Shi¹, Xiaofeng Yang², Zhefeng Gong³, Jianhua Huang⁴, Yongfeng Jin^{1*}

¹MOE Laboratory of Biosystems Homeostasis & Protection and Innovation Center for Cell Signaling Network, College of Life Sciences, ²Department of Neurosurgery, First Affiliated Hospital, School of Medicine, ³Department of Neuroscience, School of Medicine, ⁴Institute of Insect Sciences, Zhejiang University, Hangzhou, Zhejiang, ZJ310058, China

* Correspondence should be addressed to Yongfeng Jin: 0086-571-88206479(Tel); 0086-571-88206478(Fax); jinyf@zju.edu.cn(e-mail).

Supplementary information

Supplementary Tables 1, 2

Supplementary Figs. 1–11

Table S1 Specific primers used for the sgRNA		
Primer	5'-3' sequence	Assay
Ds-4-sg-F1	TTCGGGCAAGTCAGGAGCGACCCA	sgRNA for Dscam Δ 4D ^{-/-}
Ds-4-sg-R1	AAACTGGGTCGCTCCTGACTTGCC	sgRNA for Dscam Δ 4D ^{-/-}
Ds-4-sg-F2	TTCGCATATGTGTACGTGGTCGAT	sgRNA for Dscam Δ 4D ^{-/-}
Ds-4-sg-R2	AAACATCGACCACGTAACAATATG	sgRNA for Dscam Δ 4D ^{-/-}
Ds-6-sg-F1	TTCGAGTACCCTATCCCAACATTC	sgRNA for Dscam Δ 6D ^{-/-}
Ds-6-sg-R1	AAACGAATGTTGGGATAGGGTACT	sgRNA for Dscam Δ 6D ^{-/-}
Ds-6-sg-F2	TTCGACCTGGCGATTTCAGTAACT	sgRNA for Dscam Δ 6D ^{-/-}
Ds-6-sg-R2	AAACAGTTAACTGAATCGCCAGGT	sgRNA for Dscam Δ 6D ^{-/-}
Ds-9-sg-F3	TTCGGCTGATACGCAGTGGGACCT	sgRNA for Dscam Δ 9D ^{-/-}
Ds-9-sg-R3	AAACAGGTCCCACTGCGTATCAGC	sgRNA for Dscam Δ 9D ^{-/-}
Ds-9-sg-F4	TTCGGAGTCAGTCTCGTTTGGTGG	sgRNA for Dscam Δ 9D ^{-/-} and Dscam Δ 9D1 ^{-/-}
Ds-9-sg-R4	AAACCCACCAAACGAGACTGACTC	sgRNA for Dscam Δ 9D ^{-/-} and Dscam Δ 9D1 ^{-/-}
Ds-9-sg-F5	TTCGGTTATTTGGTTTATTCGGTGT	sgRNA for Dscam Δ 9D2 ^{-/-} , Dscam Δ 9D3 ^{-/-} , Dscam Δ 9D4 ^{-/-} , Dscam Δ 9D5 ^{-/-}
Ds-9-sg-R5	AAACACACCGAATAAACCAATAAC	sgRNA for Dscam Δ 9D2 ^{-/-} , Dscam Δ 9D3 ^{-/-} , Dscam Δ 9D4 ^{-/-} , Dscam Δ 9D5 ^{-/-}
Ds-9-sg-F6	TTCGTGTAAAATACAAGTTCACAG	sgRNA for Dscam Δ 9D2 ^{-/-} , Dscam Δ 9D3 ^{-/-} , Dscam Δ 9D4 ^{-/-} , Dscam Δ 9D5 ^{-/-}
Ds-9-sg-R6	AAACCTGTGAAGTTGTATTTTACA	sgRNA for Dscam Δ 9D2 ^{-/-} , Dscam Δ 9D3 ^{-/-} , Dscam Δ 9D4 ^{-/-} , Dscam Δ 9D5 ^{-/-}
Ds-9-sg-F7	TTCGCTTGCTGTTATTGGTTTATT	sgRNA for Dscam Δ 9D2 ^{-/-} , Dscam Δ 9D3 ^{-/-} , Dscam Δ 9D4 ^{-/-} , Dscam Δ 9D5 ^{-/-}
Ds-9-sg-R7	AAACAATAAACCAATAACAGCAAG	sgRNA for Dscam Δ 9D2 ^{-/-} , Dscam Δ 9D3 ^{-/-} , Dscam Δ 9D4 ^{-/-} , Dscam Δ 9D5 ^{-/-}

Table S2 Specific primers used for RT-PCR and PCR analyses		
Primer	5'-3' sequence	Assay
Ds-4-exa-F	ATATCGCGGAAAGCGGTAAATTTACAG	Examine DscamΔ4D ^{-/-}
Ds-4-exa-R	CTATACACCAACAATGCCCAAGAGTTTGTA	Examine DscamΔ4D ^{-/-}
Ds-6-exa-F	CCGAAAAGAATTGTTGCTGTAG	Examine DscamΔ6D ^{-/-}
Ds-6-exa-R	ATTGGGAAACTTGGGCGAACTCTG	Examine DscamΔ6D ^{-/-}
Ds-9-exa-F	TCTCTGAATCTATCCATATTCACATCCGT	Examine DscamΔ9D ^{-/-}
Ds-9-exa-R	GTTTCCTTGCCAAAGGACTTCGCTTTGTGC	Examine DscamΔ9D ^{-/-}
Ds-3-F	TGGATCAGGAGCGACGGTAC	RTPCR
Ds-5-R	CTCCAGAGGGCAATACCAGG	RTPCR
Ds-5-F	GCTACCAGTGCCGAACCAAAACATC	RTPCR
Ds-7-R	AGTCTCAACGCTTTTCGCCTCCAC	RTPCR
Ds-8-F	ACTTGCGTTGCCAAGAATCAGGAAG	RTPCR
Ds-10-R	GCCTTATCGGTGGGCTCGAGGATCC	RTPCR
Ac-F-q	TGTGGATATCCGTAAGGATC	QPCR
Ac-R-q	ACAGCGAAGCCAGGATGGAG	QPCR
Ds-10-F-q	TAAGGCCCTTCGCCAGGGATCC	QPCR
Ds-11-R-q	TCTCCGGGGTGTGCGCAACT	QPCR
Ds-3-F-seq	TCGTCGGCAGCGTCAGATGTGTATAAGAGACAGTGGATCAGGAGCGACGGTAC	Sequencing
Ds-5-R-seq	GTCTCGTGGGCTCGGAGATGTGTATAAGAGACAGCTCCAGAGGGCAATACCAGG	Sequencing
Ds-5-F-seq	TCGTCGGCAGCGTCAGATGTGTATAAGAGACAGGCTACCAGTGCCGAACCAAAACATC	Sequencing
Ds-7-R-seq	GTCTCGTGGGCTCGGAGATGTGTATAAGAGACAGAGTCTCAACGCTTTTCGCCTCCAC	Sequencing
Ds-8-F-seq	TCGTCGGCAGCGTCAGATGTGTATAAGAGACAGACTTTCGTTGCCAAGAATCAGGAAG	Sequencing
Ds-10-R-seq	GTCTCGTGGGCTCGGAGATGTGTATAAGAGACAGGCCCTTATCGGTGGGCTCGAGGATCC	Sequencing
Ds-10-RT	GGTTTGGGGAAGCCATCAGCCTT	RT

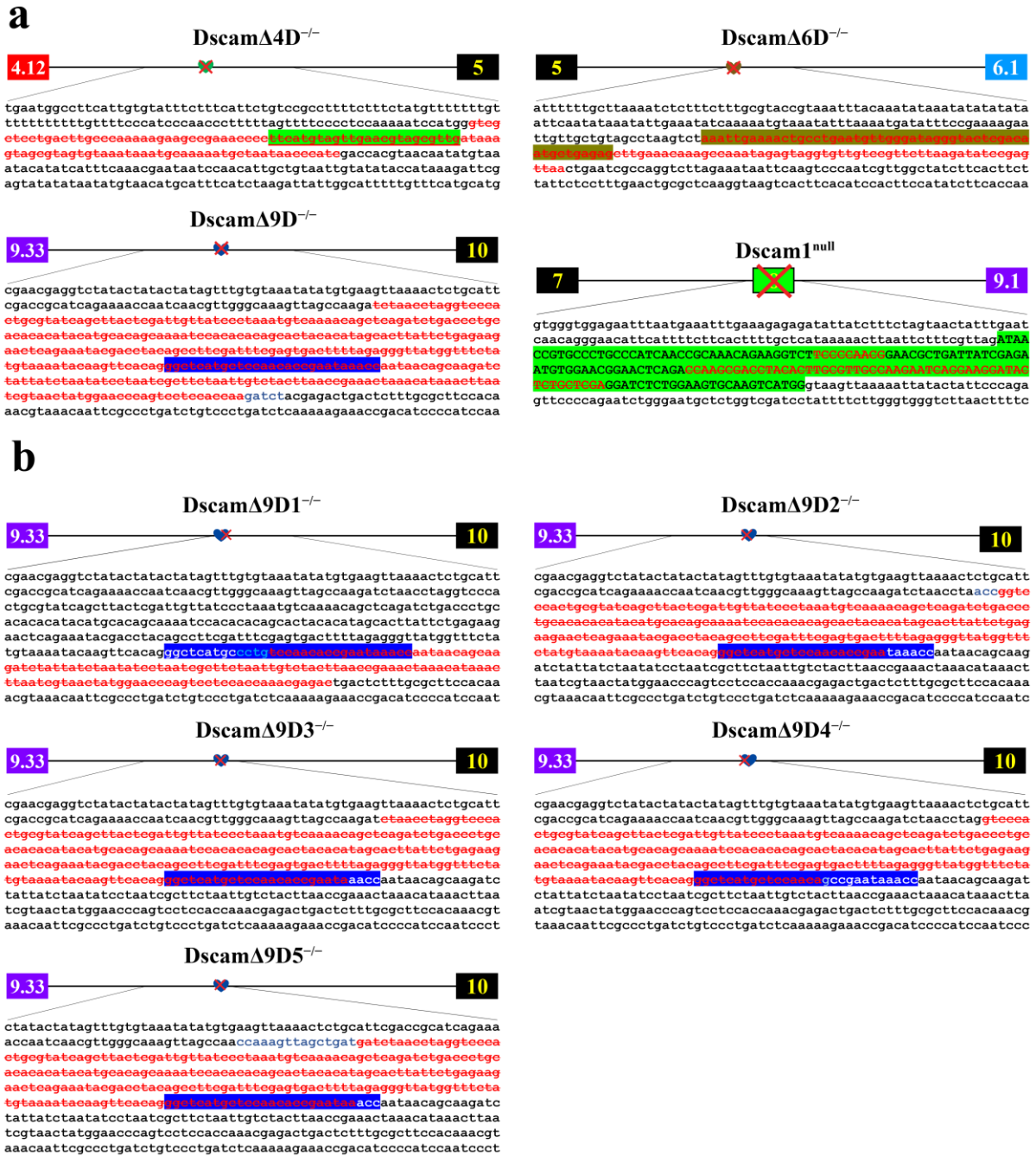


Figure S1. Schematic diagrams and deleted sequences of fly *Dscam1* mutant alleles. (a) Schematic diagrams and deleted sequences of *Dscam Δ 4D^{-/-}*, *Dscam Δ 6D^{-/-}*, and *Dscam Δ 9D^{-/-}*. The docking sequences (marked by hearts) of the exon 4, 6, and 9 clusters from the *D. melanogaster Dscam1* locus were deleted using the CRISPR/Cas9 system (designated as *Dscam Δ 4D^{-/-}*, *Dscam Δ 6D^{-/-}*, and *Dscam Δ 9D^{-/-}*). Correspondingly, we deleted the middle region of the constitutive exon 8 from *D. melanogaster Dscam1* locus (designated as *Dscam1^{null}*), which resulted in frameshift mutation (marked by a red cross). The deleted

sequences are shown in red. **(b)** Schematic diagrams and deleted sequences of $Dscam\Delta 9D1-5^{-/-}$. We used the CRISPR/Cas9 system to generate mutant flies varying the degree of deletions of the docking sequence of the exon 9 cluster (designated as $Dscam\Delta 9D1-5^{-/-}$).

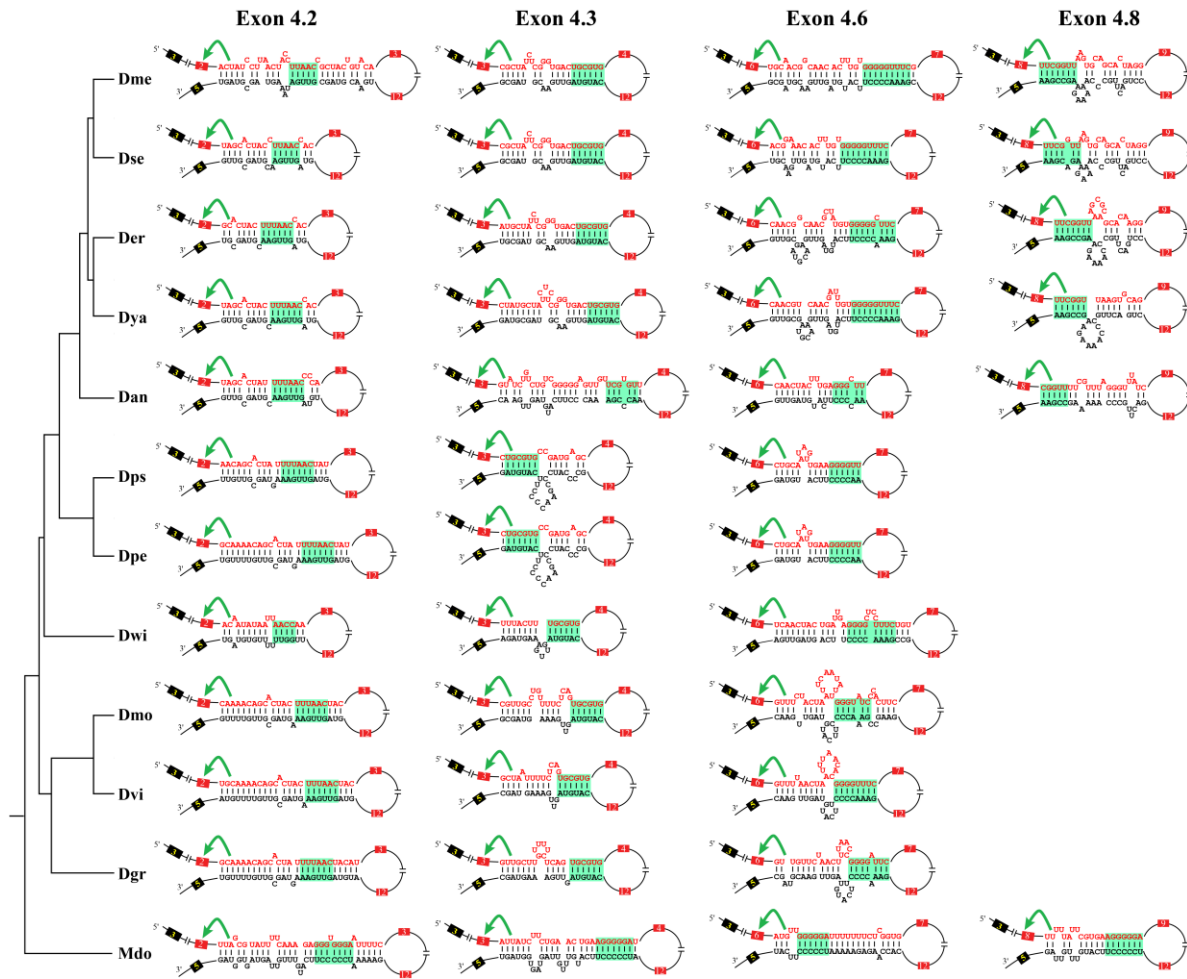


Figure S2. RNA secondary structures between the docking site and selector sequences are conserved across *Drosophila* and housefly. The base pairings between the docking site and selector sequence are conserved in exon 4.2, 4.3, 4.6, 4.8, 4.11 across *Drosophila* species and housefly. Those *Drosophila* species include *D. melanogaster* (Dme), *D. simulans* (Dsi), *D. sechellia* (Dse), *D. yakuba* (Dya), *D. erecta* (Der), *D. ananassae* (Dan), *D. willistoni* (Dwi), *D. mojavensis* (Dmo), *D. virilis* (Dvi) and *D. grimshawi* (Dgr). RNA secondary structures between the docking site and selector sequence for exon 4.11 were previously identified¹. RNA secondary structures between the docking site and selector sequence for exon 4.8 were predicted only in melanogaster group species and housefly. The sequences that make up the core of the stem are highlighted in green.

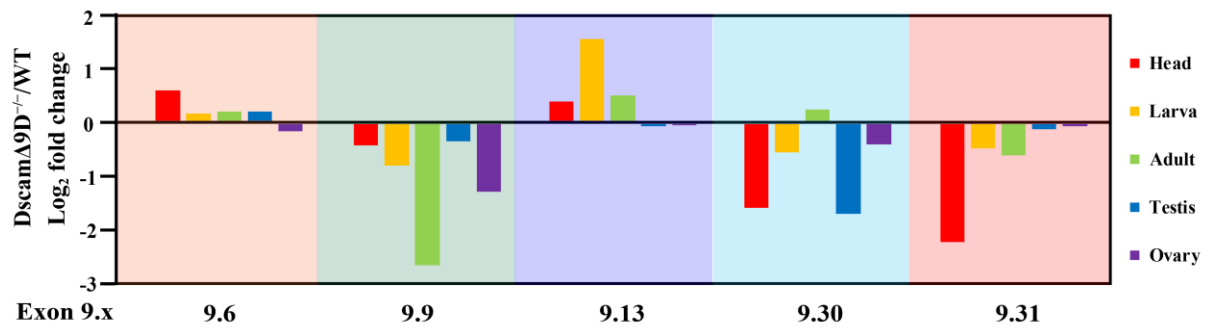


Figure S3. Deletion of the docking site led to altered frequency of the exon 9 variants.

The log₂ fold change in the frequency of most dominantly expressed variable exon 9s (exon 9.6, 9.9, 9.13, 9.30, 9.31) in various developmental stages and tissues. A relatively similar change trend of exon 9 usage was observed in various tissues of *DscamΔ9D^{-/-}*, although the alterations were subject to developmental and tissue-specific regulation.

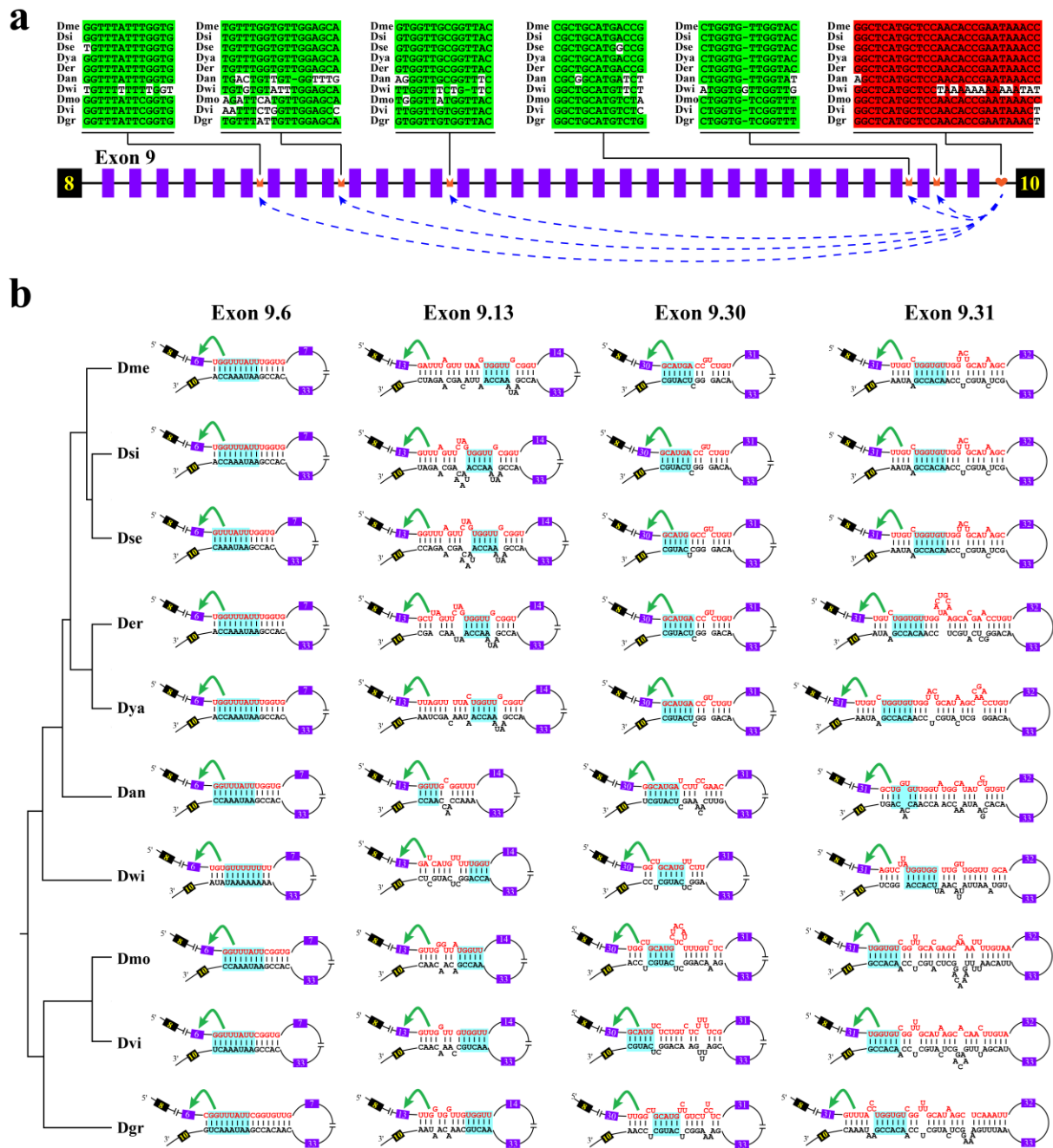


Figure S4. RNA secondary structures between the docking site and selector sequence are conserved. (a) Overview of the arrangement of the docking site and selector sequence of exon 9 cluster of *Drosophila Dscam1*. Symbols used are the same as those in Fig. 1. Constitutive exons (in black boxes), alternative exon 9s (in purple boxes), docking sites (marked by hearts) and selector sequences (marked by crowns) are shown. Above are sequences of consensus intronic elements for different species. Those *Drosophila* species include *D. melanogaster* (Dme), *D. simulans* (Dsi), *D. sechellia* (Dse), *D. yakuba* (Dya), *D. erecta* (Der), *D. ananassae* (Dan), *D. willistoni* (Dwi), *D. mojavensis* (Dmo), *D. virilis* (Dvi)

and *D. grimshawi* (Dgr). The most identical nucleotides with respect to the docking sites and selector sequences are shaded in red and green, respectively. **(b)** The base pairings between the docking site and selector sequence are conserved in exon 9.6, 9.9, 9.13, 9.30, 9.31 across *Drosophila* species. RNA secondary structures between the docking site and selector sequence for exon 9.9 were previously identified¹. The base pairings between the docking site and the selector sequences were predicted using the Mfold program². The sequences that make up the core of the stem in *Drosophila* species are highlighted in light blue.

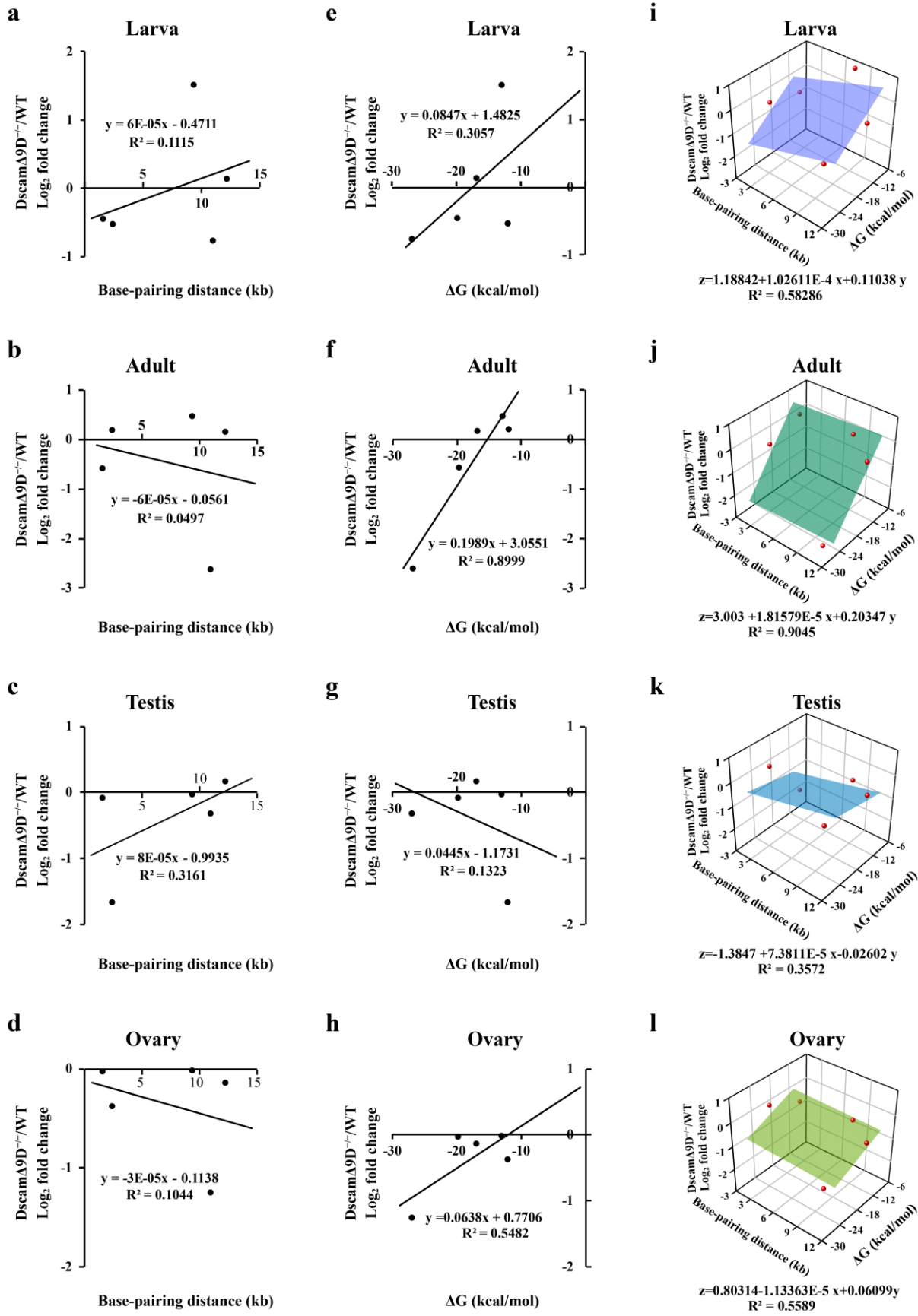


Figure S5. Deleting the docking site affected the frequency of exon 9 inclusions through disturbing the base pairing interaction in proximity- and strength-mediated manner.

(a–d) Correlation analysis between the distances of the docking site-selector interaction and the fold change in the frequency of the exon 9 variants. The distance of the docking site-selector interaction is plotted as a function of the fold change in the frequency of inclusion of the exon 9 variants in larva (a), adult (b), testis (c), ovary (d). **(e–h)** Correlation analysis between the base pairing strength (ΔG kcal/mol) of the docking site-selector interaction and the fold change in the frequency of the exon 9 variants. The strength of the base pairing between the docking site and selector sequence is plotted as a function of the fold change in the frequency of inclusion of the exon 9 variants in larva (e), adult (f), testis (g), ovary (h). **(i–l)** Multiple linear regression analysis. The combined effect of the distance and strength of the predicted docking site-selector sequence interaction is plotted as a function of the fold change in the frequency of inclusion of the exon 9 variants in larva (i), adult (j), testis (k), ovary (l). These analyses revealed a much stronger correlation of the fold change in exon 9 inclusion with the combined effect of both the distance and strength of the docking site-selector base pairing than with either its strength or distance.

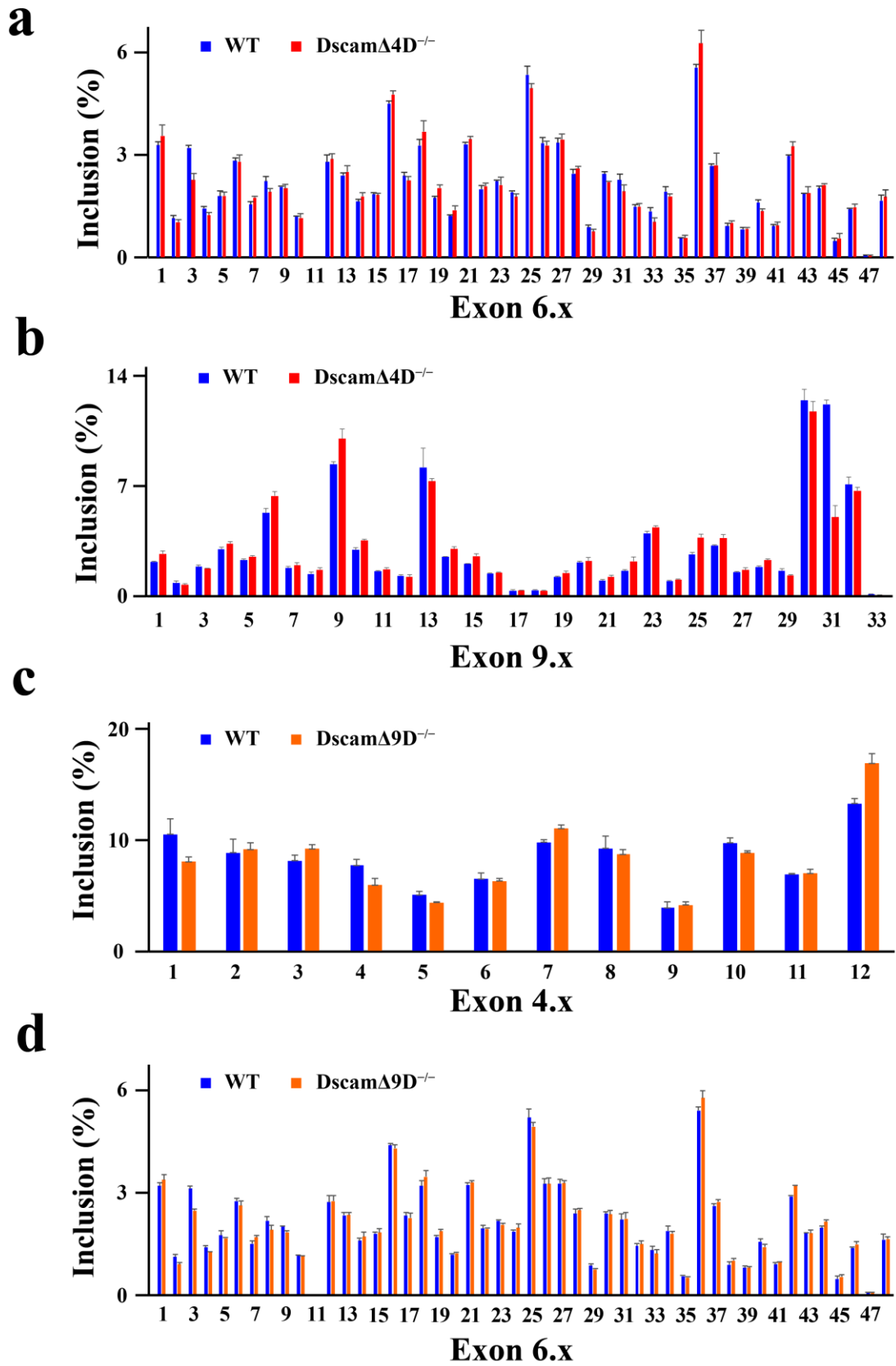


Figure S6. *Dscam* Δ 4D^{-/-} or *Dscam* Δ 9D^{-/-} flies show largely independent splicing between exon clusters 4, 6, and 9. (a) No significant differences in alternative exon 6s inclusion

between control and $Dscam\Delta 4D^{-/-}$ flies. **(b)** No significant differences in frequency of most of alternative exons 9 between control and $Dscam\Delta 4D^{-/-}$ flies were observed. **(c)** No significant differences in alternative exon 4s inclusion between control and $Dscam\Delta 9D^{-/-}$ flies. **(d)** No significant differences in alternative exon 6s inclusion between control and $Dscam\Delta 9D^{-/-}$ flies. These results indicate that alternative splicing between different clusters of *Dscam1* is largely independent.

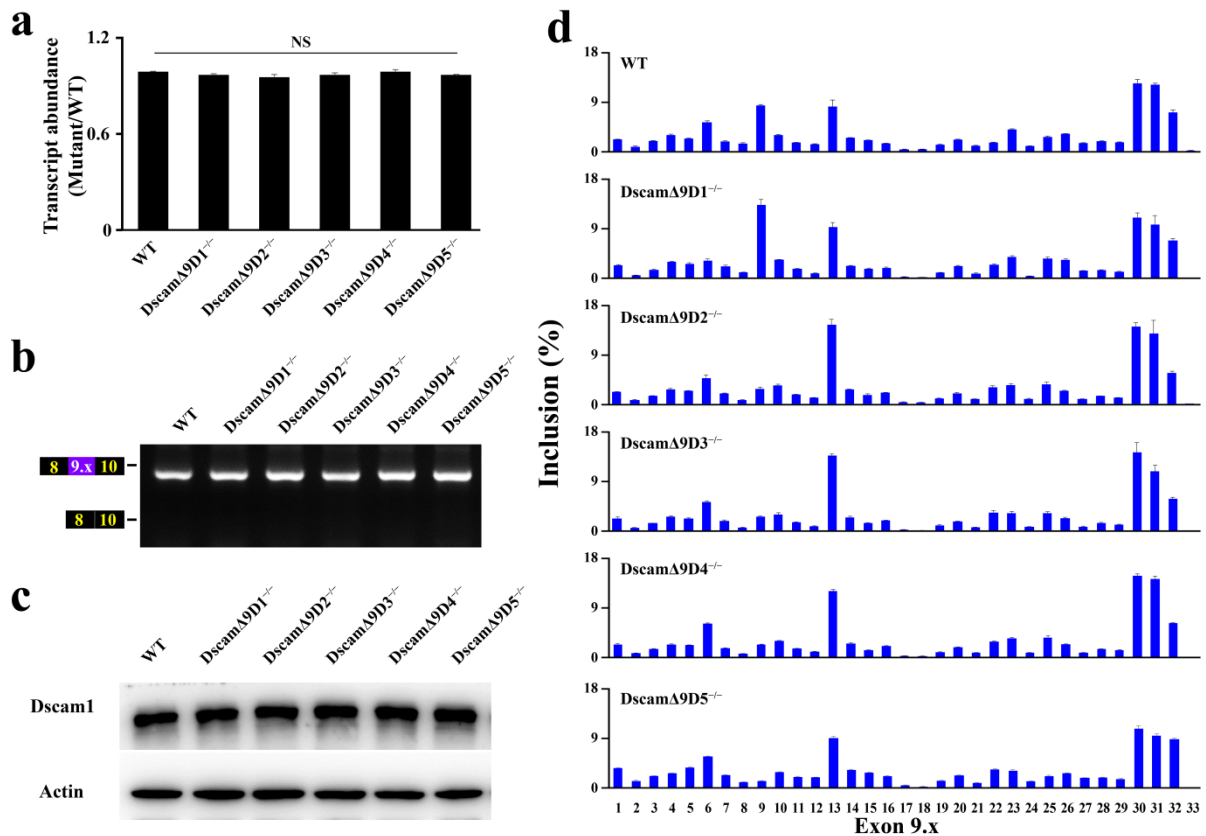


Figure S7. Molecular characterization of *Dscam*Δ9D1–5^{-/-} alleles. (a) The transcript level for each *Dscam1* mutant was indistinguishable from wild-type control; Data are expressed as mean ± s.d. from three independent experiments. *P<0.05; **P<0.01; ***P<0.001; NS, not significant (Student's t-test, two-tail). (b) The exon 9 inclusions for each *Dscam1* mutant were indistinguishable from the wild-type control. (c) Disruption of the docking sites did not affect *Dscam1* protein levels. (d) Deletion of the docking site dramatically altered the choice frequency of the exon 9 variants. The relative frequency of the exon 9 inclusion in wild type and mutants was shown (from exons 9.1 to 9.33).

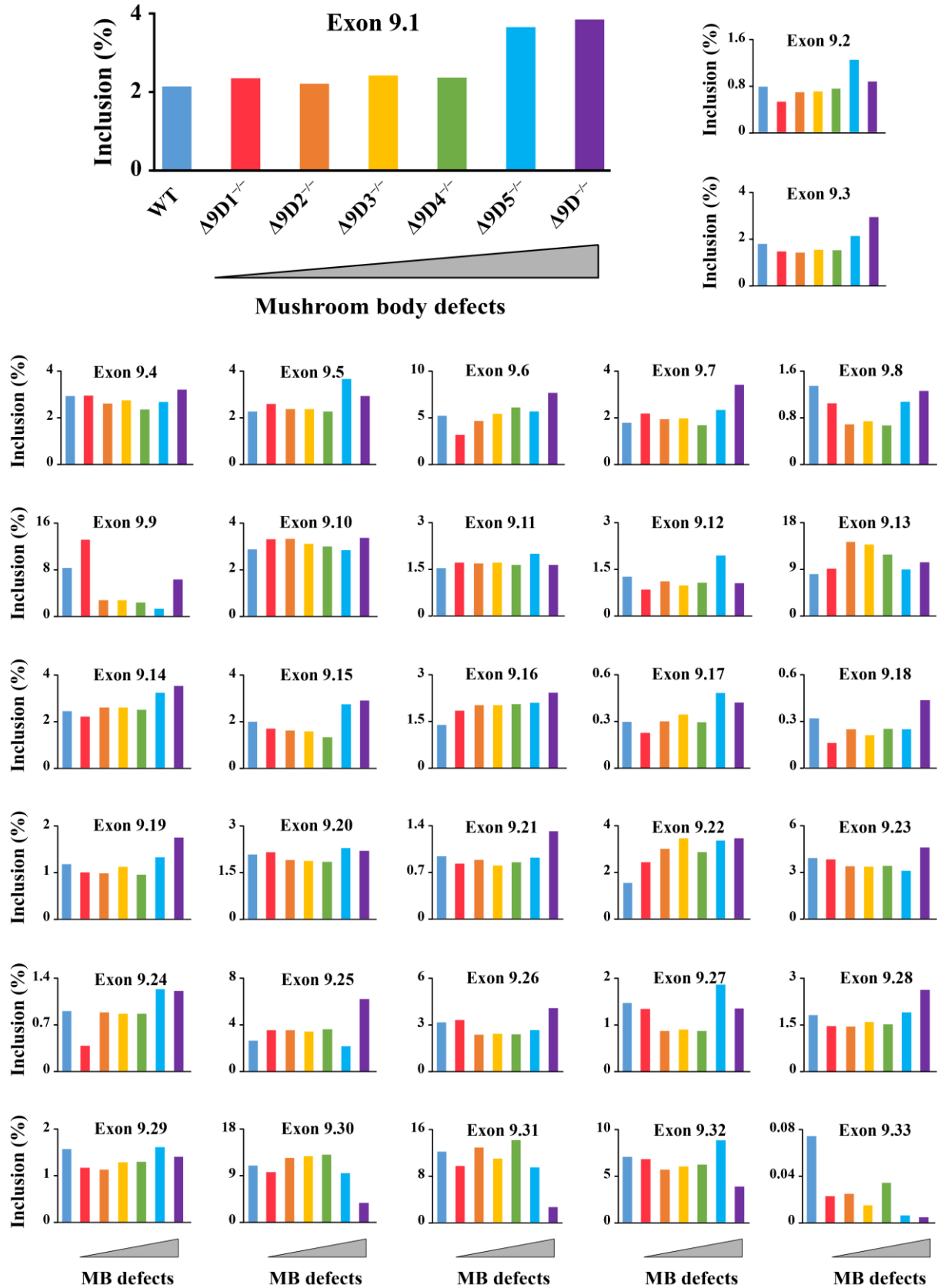


Figure S8. Analyses of correlation of the expression of specific exon 9 variants with mushroom body (MB) defects. The histograms show the relationship between inclusion of

exon 9 and the proportion of mutant mushroom body defects. Different colors represent different mutants (light blue: wild type, red: $Dscam\Delta 9D1^{-/-}$, orange: $Dscam\Delta 9D2^{-/-}$, yellow: $Dscam\Delta 9D3^{-/-}$, green: $Dscam\Delta 9D4^{-/-}$, sky blue: $Dscam\Delta 9D5^{-/-}$, purple: $Dscam\Delta 9D^{-/-}$). Mutants were arranged from low to high proportion of mushroom body defects. In order to show the inclusion of each exon 9 variants in different mutants, exons 9.1 to 9.33 are represented by different graphs. As shown in the figure, the inclusions of almost all exons have been changed.

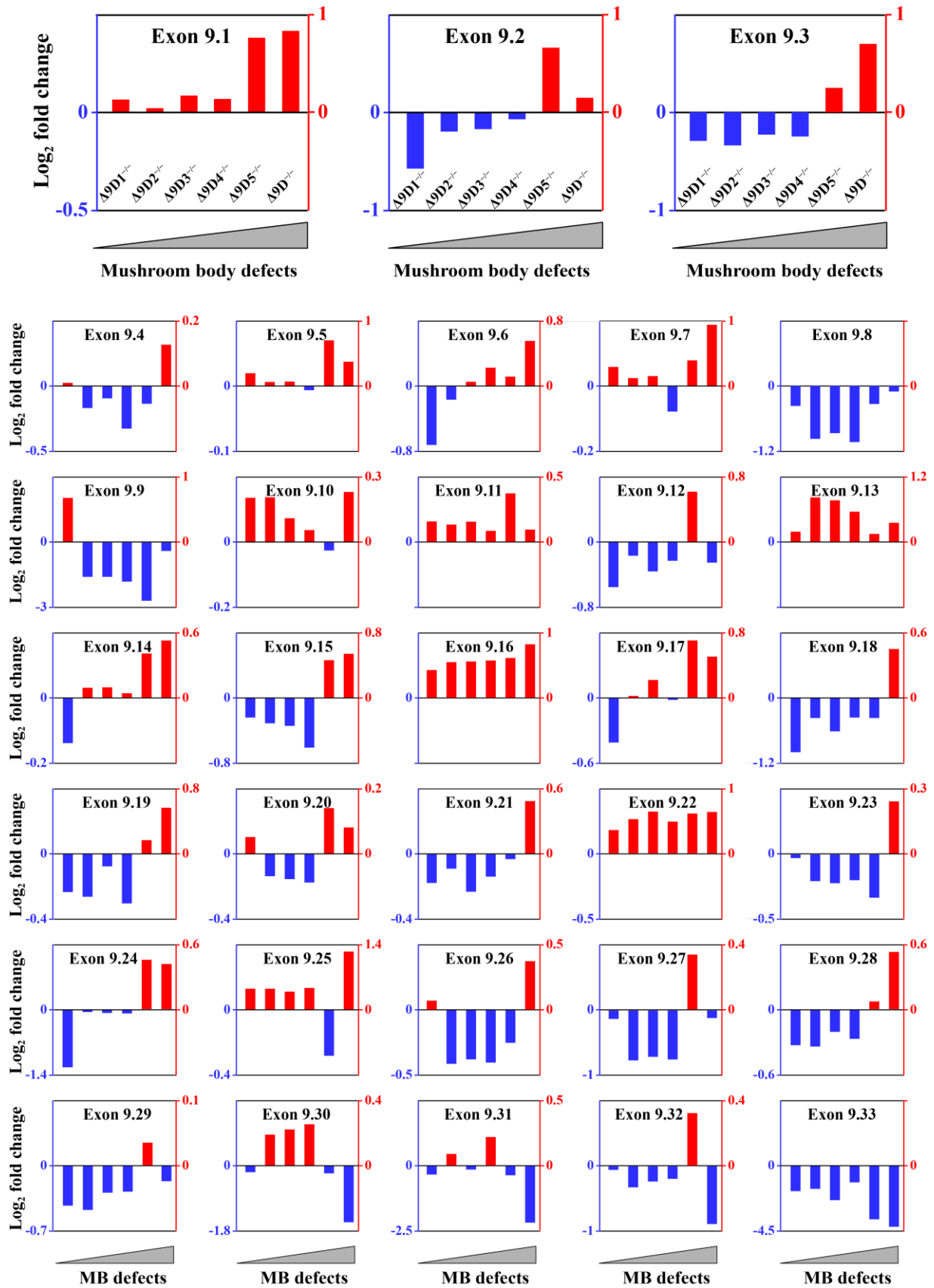


Figure S9. Analyses of correlation of the expression changes of specific exon 9 variants with mushroom body (MB) defects. The log₂ fold change of each mutant construct

compared to wild type is represented as column chart. Mutants were arranged from low to high proportion of mushroom body defects. In order to show the changes in each exon 9 variants with different mutants, exons 9.1 to 9.33 are represented by different graphs. As we can see from the figures, the inclusions of almost all exons have been changed.

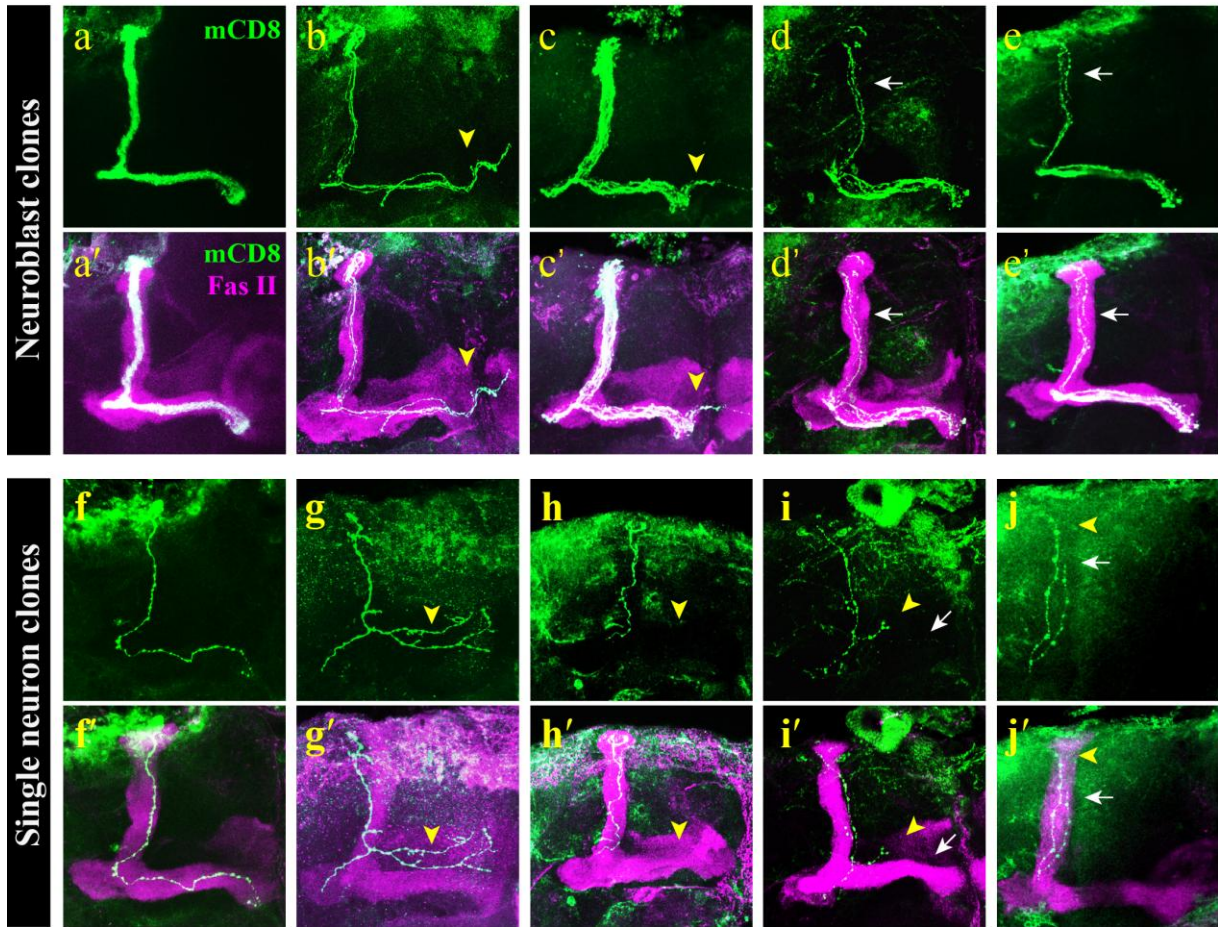


Figure S10. Phenotypic analysis of *Dscam1* mutant mushroom body axons at neuroblast and single-cell clones (supplemental to Figure 7c-f', h-k'). All drawings and images (a-j') are adult mushroom body of brain hemisphere. a-j are the same as a'-j', respectively, showing FasII staining. The control neuroblast clones show the bifurcated axon with a dorsally and a medially running branch, while *Dscam* Δ 4D^{-/-} and *Dscam* Δ 9D^{-/-} mutant clones exhibited either a growth defect or a guidance axonal defect, or sometimes a combination of the growth and guidance defects. (a-e') Wild type and mutant mushroom body axons in neuroblast (NB) clones (supplemental to Figure 7c-f'). Compared with wild-type neuroblast (NB) clones (a, a'), mutant NB clones display overextension of axon branches (b, b', c, c'), thinning and thickening of α/β axon branches (d, d', e, e'). Yellow arrowhead indicated growth defect that axon branches extended beyond the ends of β lobes (b, b', c, c'). White arrowhead indicated guidance defect that axons in α lobe was thinner than in wild-type control (d, d', e, e'). (f-j') Wild-type and mutant mushroom body axons in single neuron clones (supplemental to Figure 7h-k'). Unlike wild type single neuron clones (f, f'), mutant clones exhibited either growth (g,

g', h, h'), or a combination of growth and guidance defects (i, i', j, j'). Supernumerary branches (g, g') or an unusual single-branch phenotype with no axon bifurcation at the peduncle end (h, h') were shown in some single-cell clones (yellow arrowhead). In panel i and j, yellow arrowhead indicates growth defect, while white arrowhead represents guidance defect.

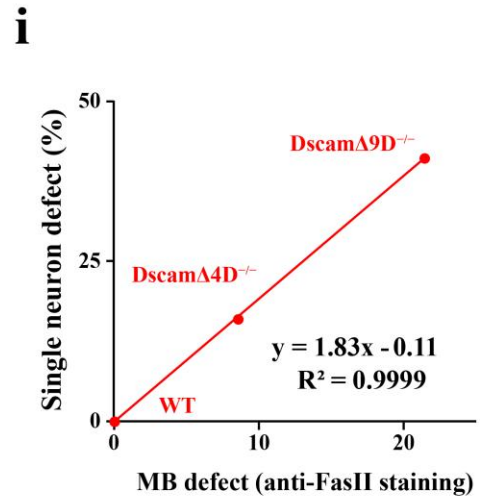
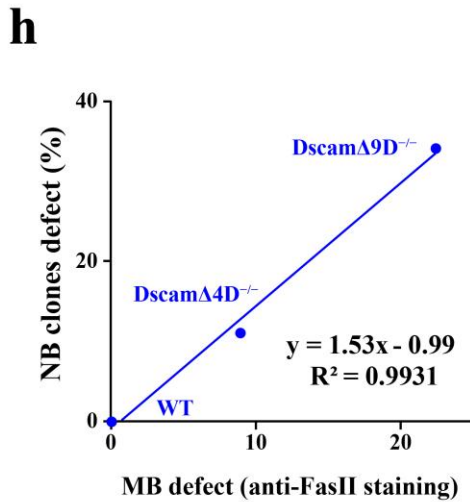
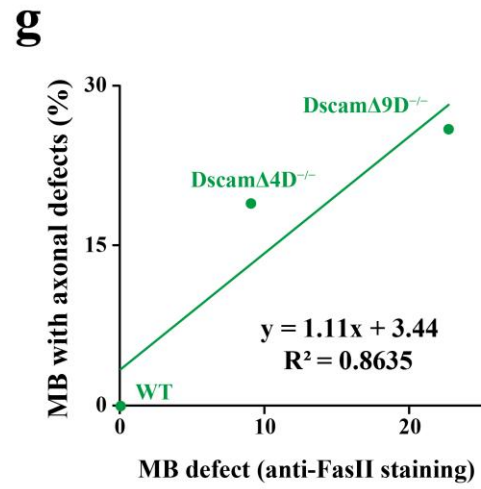
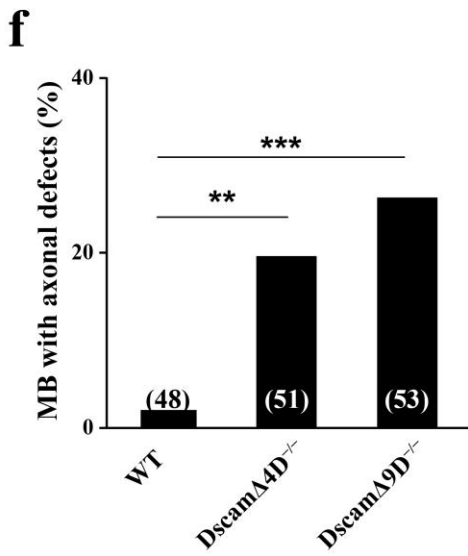
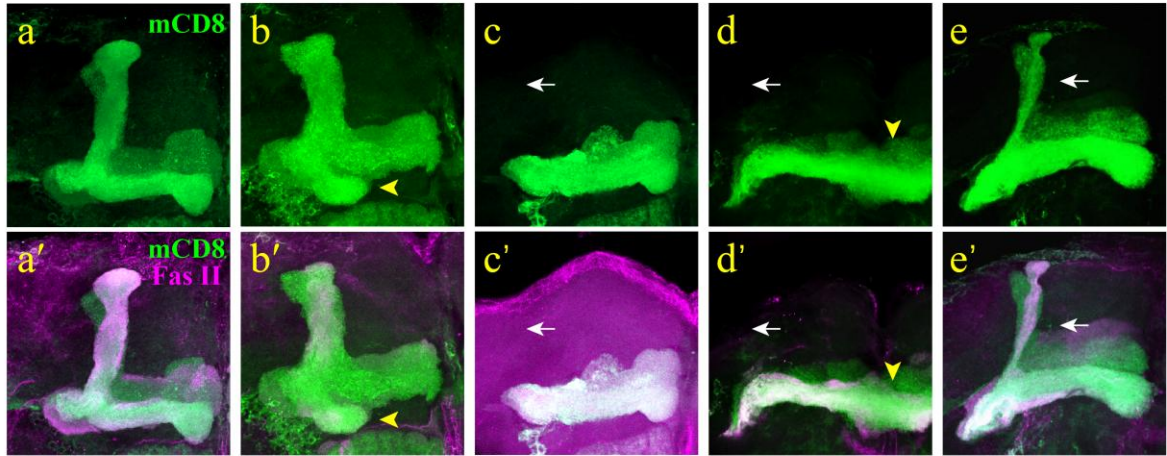


Figure S11. Phenotypic analysis of *Dscam1* mushroom body axons in isogenic mutant brains. (a–e') Wild type and mutant axons in large neuroblast (NB) clones. All drawings and images (a–e') are adult mushroom body of brain hemisphere. a-e are the same as a'-e',

respectively, showing FasII staining. A control neuroblast clones show the bifurcated axon with a dorsally and a medially running branch, while $Dscam\Delta 4D^{-/-}$ and $Dscam\Delta 9D^{-/-}$ mutant clones exhibited either a growth defect or a guidance axonal defect, or sometimes a combination of the growth and guidance defects. Compared with wild-type neuroblast (NB) clones (a, a'), mutant NB clones display growth (b, b'), and guidance (c, c', e, e') defects, or sometimes a combination of them (d, d'). Yellow arrowhead indicated growth defect that axons did not reach the ends of α/β lobes in some mutant clones (yellow arrowhead, b, b', d, d'). White arrowhead indicated guidance defect that axons in α lobe was thinner than in wild-type control or lost (white arrowhead, c, c', e, e'). **(f)** Quantification of mushroom body axonal defects in isogenic mutant brains. **(g–i)** Correlation of mushroom body defects detected by anti-FasII staining with axonal defects observed in isogenic mutant brains (g), neuroblast clones (h), or single neuron clones (i).

References

1. Yang Y, *et al.* RNA secondary structure in mutually exclusive splicing. *Nat Struct Mol Biol* **18**, 159-168 (2011).
2. Zuker M. Mfold web server for nucleic acid folding and hybridization prediction. *Nucleic Acids Research* **31**, 3406–3415 (2003).
3. Crooks GE, Hon G, Chandonia JM, Brenner SE. WebLogo: a sequence logo generator. *Genome Res* **14**, 1188-1190 (2004).